PCCP

Accepted Manuscript

ROYAL SOCIETY OF CHEMISTRY

www.rsc.org/pccp

Nanolubrication by ionic liquids: molecular dynamics simulations reveal an anomalous effective rheology

Nicolas Voeltzel[1,2], Andrew Giuliani[1], Nicolas Fillot[1], Philippe Vergne[1] and Laurent Joly[2]*

1) Laboratoire de Mécanique des Contacts et des Structures, UMR5259 INSA de Lyon-CNRS, Université de Lyon, 69621 Villeurbanne, France

2) Institut Lumière Matière, UMR5306 Université Lyon 1-CNRS, Université de Lyon, 69622 Villeurbanne, France

*Corresponding author: laurent.joly@univ-lyon1.fr

Abstract

This article describes molecular dynamics simulations of an ionic liquid (IL) confined between iron oxide surfaces under relatively high pressure and severe shearing, representative of a typical steel-steel lubricated contact. The simulations reveal the presence of hydrodynamic and thermal slip at the walls, despite the wetting nature of the fluid/wall interface. A crucial consequence of the temperature slip is the subsequent increase of the fluid temperature under shear, which modifies its effective rheology, resulting in a saturation of the shear stress at high shear rates. Overall, this article provides a methodology for accurate modeling of tribological contacts lubricated by a nanometer-thick IL film. The results contribute to the debate on the saturation of the shear stress at high shear rates, and reveal the rich phenomenology arising in severe tribological conditions, departing from the traditional understanding of nanofluidic transport, mainly built in the linear response regime and standard thermodynamic conditions.

1. Introduction

Room temperature ionic liquids (RTILs), often simply referred to as ionic liquids (ILs), are salts composed of atomic or molecular cations and anions. Although these compounds are subjected to strong Coulombic interactions, they are liquid over a wide range of temperature (from well below 0 °C to hundreds of Celsius degrees)[1,2]. It is possible to adjust the physical and chemical properties of RTILs by choosing or modifying the appropriate cation or anion. A large number of combinations is possible, with some estimates reaching 10^{18} couples[1]. In engineering problems, ILs are considered as promising lubricants due to the diversity of their characteristics, and their favorable response in lubricated interfaces[3–5]. Consequently, in the last decade, the interest in ILs as lubricants has developed quickly, as evidenced by the increasing number of papers published each year on the subject[3].

In a lubricated contact subject to severe solicitations, the heat produced by friction can cause an important increase of temperature. In addition to a significant thickness reduction, this may lead to the degradation, evaporation, and even combustion of the lubricant[5]. ILs feature several favorable characteristics that can prevent those undesired situations, including high thermal stability, non-flammability, negligible volatility, and appropriate pressure-viscosity and temperature-viscosity dependences[3,5–7]. ILs were also suggested as lubricants in spatial applications owning to their low vapor pressure and high radiation resistance properties[8]. They were as well considered in lubricated systems for their use as additives[3] or with additives[5] and can exhibit in both cases better responses than usual lubricants.

Simultaneously, the thickness of lubricated contacts has gradually decreased due to more demanding design, and environmental / efficiency constraints[9]. As a consequence, the lubricant film thickness of such systems has been reduced down to the size of a few molecules at some locations, where the fluid can no longer be considered as a continuum medium. The discrete conformation of the molecules induces a unique rheology and a specific interfacial behavior which will have a significant impact on the global response of the contact to operating solicitations[10]. Detailed investigations on ILs as lubricants at the nanoscale are thus essential to anticipate future lubricated systems.

Numerous experimental studies at macroscale emphasized the influence of ILs composition on their intrinsic properties and tribological response. First notable observation, the alkyl chain length of the ions has a direct influence on the ILs viscosity[1,3], on their melting point[3] and on their surface tension and pressure-viscosity coefficients[11]. Similarly, anion and cation composition and structure directly affect the same intrinsic properties[3,7,11,12] together with friction and wear[1,13–15]. The influence of both ionic liquid composition and surface nature on tribofilm formation, lubricant squeeze-out, surface corrosion and wear[16] was also evidenced experimentally. Questions then arose about the replication of all the above-mentioned effects at smaller scale and, more generally, about the influence of each nanoscale feature on the global system response. ILs nanoconfinement implies a structuration of the ions in layers next to the surfaces, which depends first on the surface charge, as well as a change of the global dynamics. Numerical and experimental works revealed that over positively or negatively charged walls stand anion or cation monolayers[17], respectively, and over neutral surfaces stand mixed cation/anion layers[18,19]. Ions size also impacts structuration: a typical example is the formation of tail-to-tail bilayers of cations if their alkyl chain length is oversized[20].

Although few works were conducted in the field, studies based on molecular dynamics (MD) simulations depicted the featured mass transfer of the confined ions[21,22] and the effect of surface roughness[23]. At a larger scale, the effects of nanoconfinement on the contact dynamics can be measured through the influence of different parameters on the overall friction response of the system. Different experimental research groups thus revealed the primary role of the fluid layering and its thickness on the global viscosity of the confined ILs[24]. Similarly, under severe confinement (e.g. a few layers of ions subjected to high pressure), a complex relationship between shear rate and the ensued friction was characterised[24]. In the most extreme conditions, ILs layer(s) confined between shearing surfaces can even exhibit a solid-like behavior[15,25]. MD allows a detailed exploration of the physical phenomena occurring at high confinement and therefore it is an appropriate tool for elucidating the tribological properties of complex fluids. It also can properly model the distinct polar nature of oxide surfaces (composed of charged atoms), and characterize their interactions with lubricants, and in particular with ionic liquids.

Finally, among the works conducted on nanoconfined ILs and the few ones on their response to shearing, none simulated surfaces representative of a classical steel-steel contact. One of the goals of this work is thus to characterize the behavior of a nanoconfined sheared IL in between FeO solid walls, under the typical working conditions of a lubricated contact. Introducing the influence of these realistic surfaces to explore the IL behavior when the contact is static or under shearing would contribute to improve the current knowledge on a new class of promising lubricants. A second aspect poorly investigated so far, to the best of our knowledge, is the thermal distribution in sheared ILs, whereas severe degradations might result from an immoderate heating. In this paper, we therefore show how a reliable MD model can predict the intrinsic properties of a RTIL in good agreement with measurements. Confinement and shearing conditions are then simulated: the occurrence of layering at the interface and its consequence on friction are discussed thanks to a through-thickness mass and energy transfer analysis.

2. Model

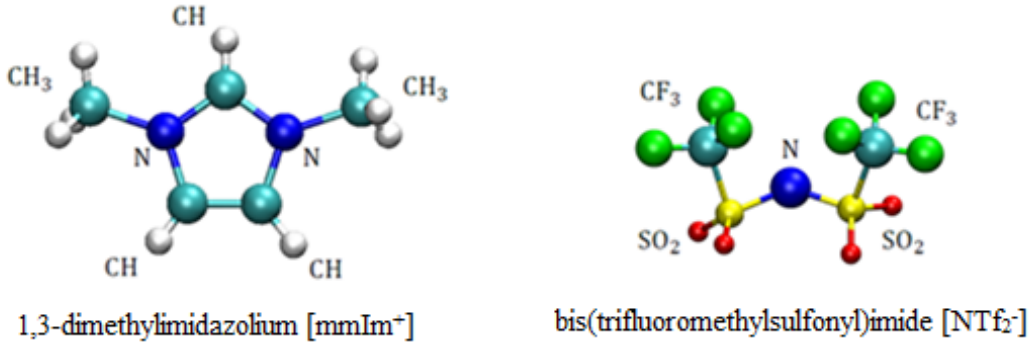

Figure 1. *Simulated Ionic Liquid: cation (left) and anion (right) molecules.*

In the context of mechanical transmission, RTILs were experimentally studied in steel-steel contacts, as it is frequently the case in lubricated systems. Under such conditions, it was observed that hydrophobic anions like bis(trifluoromethylsulfonyl)imide [NTf_2^-] perform well[3]. Moreover ILs with this anion exhibit pressure-viscosity coefficient and viscosity index ratio[7,11] that confer them an optimum stability under high pressure and wide-temperature range conditions. With respect to the cation, imidazolium-based RTILs proved to be thermally stable and adaptable. Indeed, through different chemical reactions, alkyl chains of varying lengths can be positioned on the imidazole ring, modulating its physical and chemical characteristics[5]. Finally, coupling a

bis(trifluoromethylsulfonyl)imide [NTf_2^-] anion with a short alkyl chain length imidazolium as the 1-3 dimethylimidazolium [$mmIm^+$] (illustrated in Fig.1) results in an ionic liquid with one of the lowest possible viscosity, and comparable to the one of common lubricants[3,11]. This feature can induce low friction in tribological systems working in the full film lubrication regime, but also cause more lubricant squeezing out of the contact, which would highly favor the presence of the nano-confined areas that are central in this work. At last, the size of [$mmIm^+$] cations is very close to the one of [NTf_2^-] anions, meaning the results of this study are exempt from possible asymmetrical effects. To model the behavior of ionic liquids by MD simulations, Canongia Lopes *et al.*[26,27] built a non-polarizable all-atom force field from quantum mechanical calculations. This force field is able to describe a large set of IL compounds, but it generally fails to reproduce quantitatively their transport properties. In particular, it typically overestimates their viscosity by one order of magnitude[28]. As quantitative results were expected from the present study, we implemented a standard charge scaling procedure[28,29] in order to properly reproduce the evolution of the density and of transport properties of the [$mmIm^+$][NTf_2^-] ionic liquid with the temperature. This modification was conducted following the method described by Chaban[30] and is described in detail in Electronic Supplementary Information (ESI).

The surface of carbon steel in contact with ambient air oxidizes and different compounds can result from the reaction (FeO, Fe_2O_3, FeO(OH)...)[31]. Among those compounds, iron oxide (FeO) is a relevant candidate to realistically describe the upper molecular layers of an engineering surface. The ionic liquid was thus confined between two model FeO surfaces. The integration of FeO in MD simulations was ensured by a force field proposed by Cygan *et al.*[32] and later validated for metal oxides[33]. Only intermolecular interactions were employed in this force field to represent the solid. The values of the Lennard-Jones coefficients were used as they were in the original force field but the Coulombic charges were set to the fully ionized values of the atoms: -2.e for the oxygen atoms and +2.e for the iron ones, so as to better capture the polarity of FeO surfaces, and its effect on the confined IL. Further to this adjustment, the relative deviation between the modeled crystal lattice constant and its theoretical value was less than 3.4%. Full details of the force field used in this work are available in ESI.

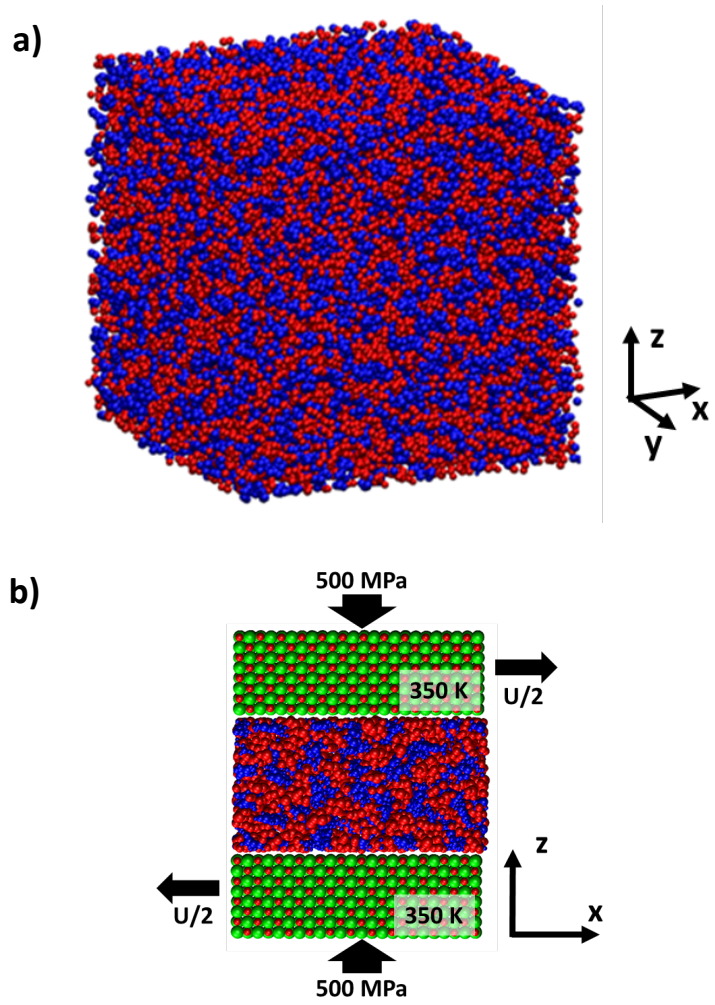

Figure 2. *Simulation domains of a) the bulk IL with 3 periodic boundaries (50x50x50 Å^3) b) the confinement of 188 IL pairs between two FeO walls with periodic boundaries along x and y (50x50 Å²). Cations atoms are in blue and anions ones are in red. In the FeO walls, Fe atoms are in green and O atoms in red.*

Molecular Dynamics (MD) simulations were conducted with the open source LAMMPS code[34]. A cuboidal simulation cell (Fig.2a) was defined and periodic boundary conditions applied along x and y directions. In the first simulations of the bulk IL properties, periodic boundary conditions were also applied along the z axis, and the dimensions of the numerical domain in all directions were equal to 50 Å. In the case of the confined IL simulations (Fig.2b), the thickness of the iron oxide walls was set to 8 atom layers (corresponding to about 16 Å). The ionic liquid thickness was free to evolve according to the number of molecules in the simulations and to the imposed conditions (temperature, pressure, wall velocity…).

To optimize computational times, the RESPA algorithm[35] was used to integrate Newton's equation of motion over different time steps depending on the considered interaction forces. Integration time step was set to 0.5 fs for intramolecular interactions and to 2 fs for intermolecular ones. During the relaxation stage of equilibrium simulations with the IL alone, Nose-Hoover barostat and thermostat regulated the pressure and temperature of the fluid with relaxation times of 2000 fs and 200 fs, respectively. When the IL was confined by solid walls, only the temperature of the surfaces was held constant with a Langevin thermostat[36] and the IL temperature was let free to evolve. The pressure was imposed through a normal force uniformly applied to the atoms located at the wall surfaces not in contact with the fluid (Fig.2b). In order to depict as well as possible a realistic tribological contact, pressure was set to 500 MPa and the wall temperature to 350 K.

3. Results and discussion

3.1 Bulk ionic liquid: viscosity

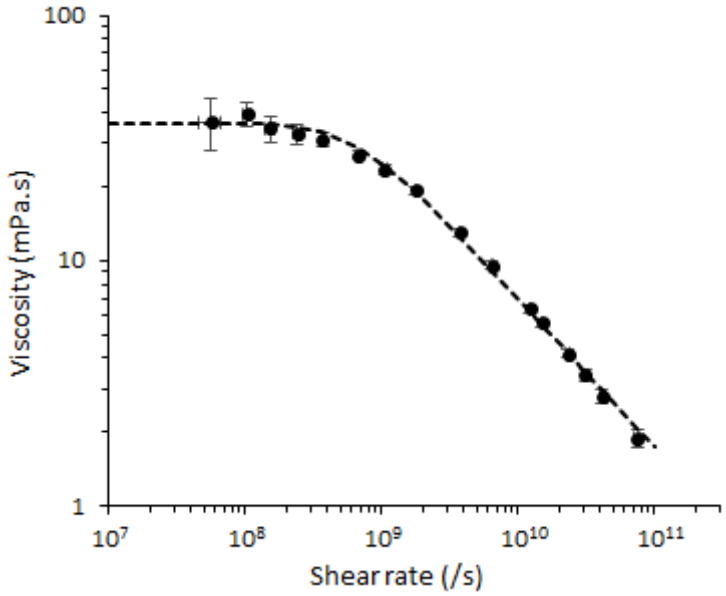

Figure 3. *Dependence of the bulk shear viscosity of [mmIm$^+$][NTf$_2^-$] on shear rate at T = 303 K and p = 0.1 MPa, obtained from MD simulations (circles). Results are fitted with a Carreau law, Eq. (1), with η_N = 36 mPa.s, t_{rel} = 1.48 ns and N = 0.302 (dashed line).*

Simulations were first carried out to compute the variation of the bulk shear viscosity η_{bulk} of [mmIm$^+$][NTf$_2^-$] with shear rate at *T* = 303 K and p = 0.1 MPa. Muller-Plathe algorithm[37] was used

to ascertain the viscosity: momenta between particles belonging to different regions of the simulation domain were exchanged at regular time steps to introduce shearing between those regions. This way, viscosity was calculated over 4 orders of magnitude of shear rate. This approach is limited down to a certain shear rate value because the hydrodynamic velocity of the atoms becomes too low to be properly detected owing to the relative increase of the thermal noise. Results obtained for η_{bulk} are plotted on Fig.3, where they are fitted with a Carreau model[38]:

$$\eta_{bulk} = \eta_N \left(1 + (\dot{\gamma} t_{rel})^2\right)^{\frac{N-1}{2N}} \quad (1)$$

where $\dot{\gamma}$ is the shear rate, η_N the Newtonian viscosity previously calculated in the low shear rate limit using a Green-Kubo expression (η_N = 36 mPa.s), t_{rel} the relaxation time and N the exponent of the Carreau expression. The two latter parameters were evaluated from a nonlinear regression and found to be equal to 1.48 ns and 0.302, respectively. We observed that the numerical values were well represented by the Carreau model. The Newtonian plateau, corresponding to the Newtonian viscosity, was reached in the simulations. A classical viscosity drop was observed beyond the plateau, with the fitted relaxation time t_{rel} = 1.48 ns close to the molecular relaxation time, estimated to ca. 2 ns from the equilibrium IL properties by using the following expression:

$$t_{rel} = d^2/D \quad (2)$$

where D is the average diffusion coefficient (at T = 303 K and p = 0.1 MPa) and d the typical ion size.

3.2 Confined ionic liquid: structuration and orientation

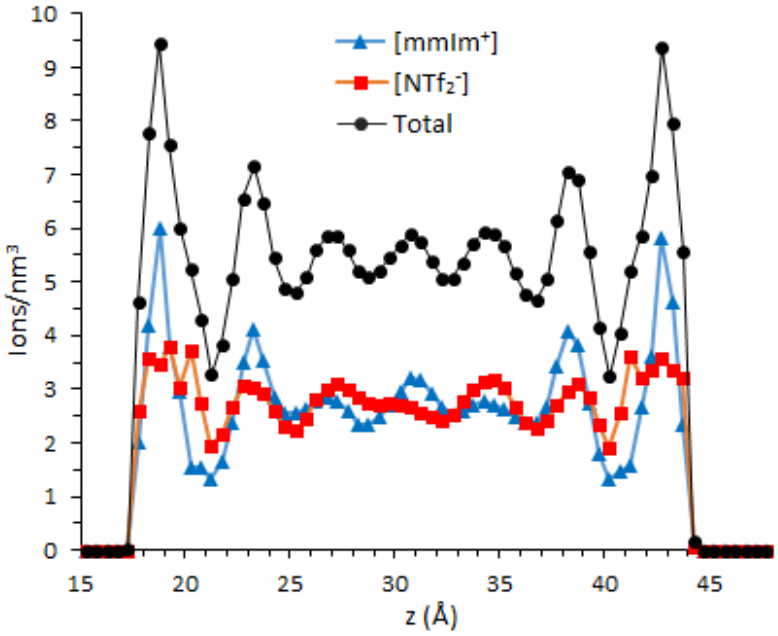

Figure 4. *Ion number density profiles of the [mmIm$^+$][NTf$_2^-$] IL confined between FeO surfaces with a pressure p = 500 MPa and a wall temperature T = 350 K: [mmIm$^+$] cations (blue triangles), [NTf$_2^-$] anions (red squares), and total density (grey circles).*

When it was confined between two surfaces, the ionic liquid lost its homogeneous structure with respect to the direction perpendicular to the walls. Fig.4 shows the ion density profiles[a] of 188 [mmIm$^+$][NTf$_2^-$] pairs confined in between two FeO surfaces at *T* = 350 K and under a pressure p = 500 MPa. The resulting film thickness was 28.4 Å. Well-defined ion layers were observed close to the surfaces, with first density peaks reaching ca. 220 and 135 % of the bulk density for the cations and anions, respectively. Both cations and anions were well represented in every formed layer, implying that no monolayer of a single ionic type was present at the interface. The amplitude of the layers density declined with the distance from the walls, and almost vanished after two occurrences. Thus, the average density in the central region of the confinement was very close to the IL bulk one.

[a] To compute the density profiles, all the atoms belonging to a given ion type were binned along the z direction, and the resulting profile was then normalized by the number of atoms per ion type.

The organization of the simulated solid material can explain the absence of separated layers of cations or anions: even though the studied surfaces were polar, including both iron (2+) and oxygen (2-) ions, and so subject to Coulombic interactions, they remained globally uncharged and their first atomic layer in contact with the fluid was equally composed of alternating Fe and O ions. The distance between Fe and O ions in the solid being significantly smaller than the size of IL ions, the latter did not experience a net Coulombic attraction/repulsion and could mix freely near the surfaces. The formation of mixed anion-cation layers was also proven experimentally for ILs confined between neutral, apolar graphitic or gold surfaces[18,19], and numerically between iron surfaces[39] whereas successive monolayers of separated cations and anions were distinctly observed next to negatively charged surfaces like mica[24,40].

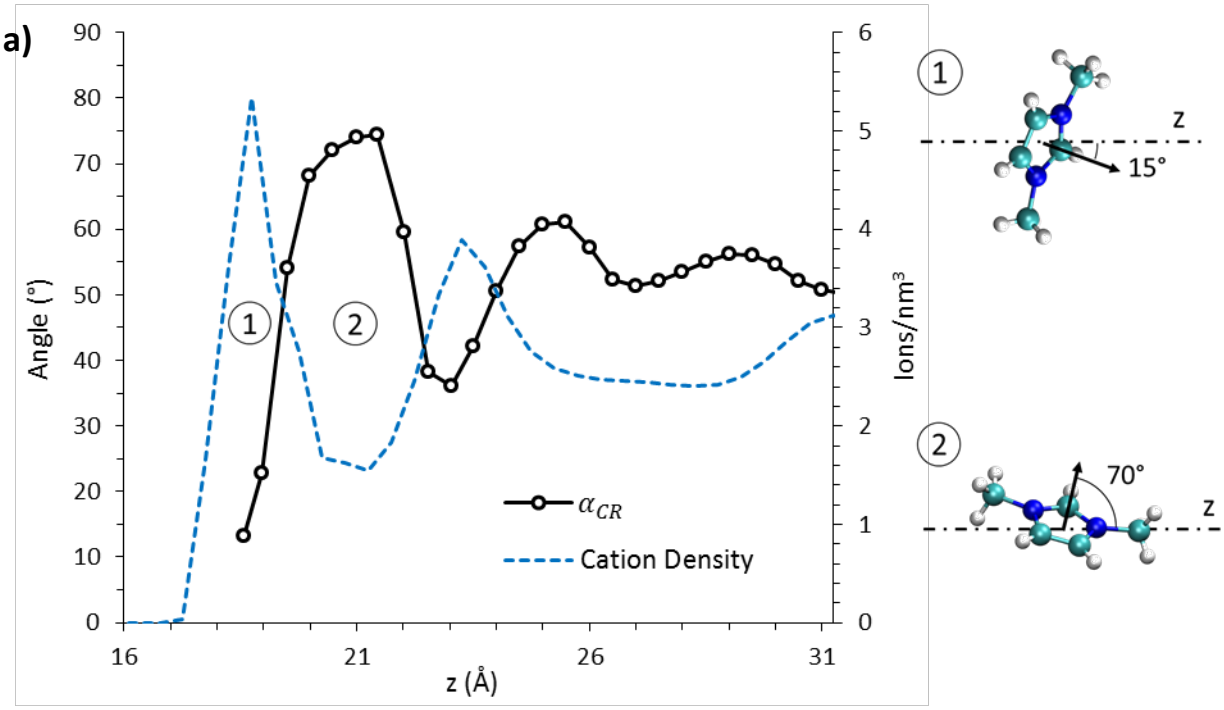

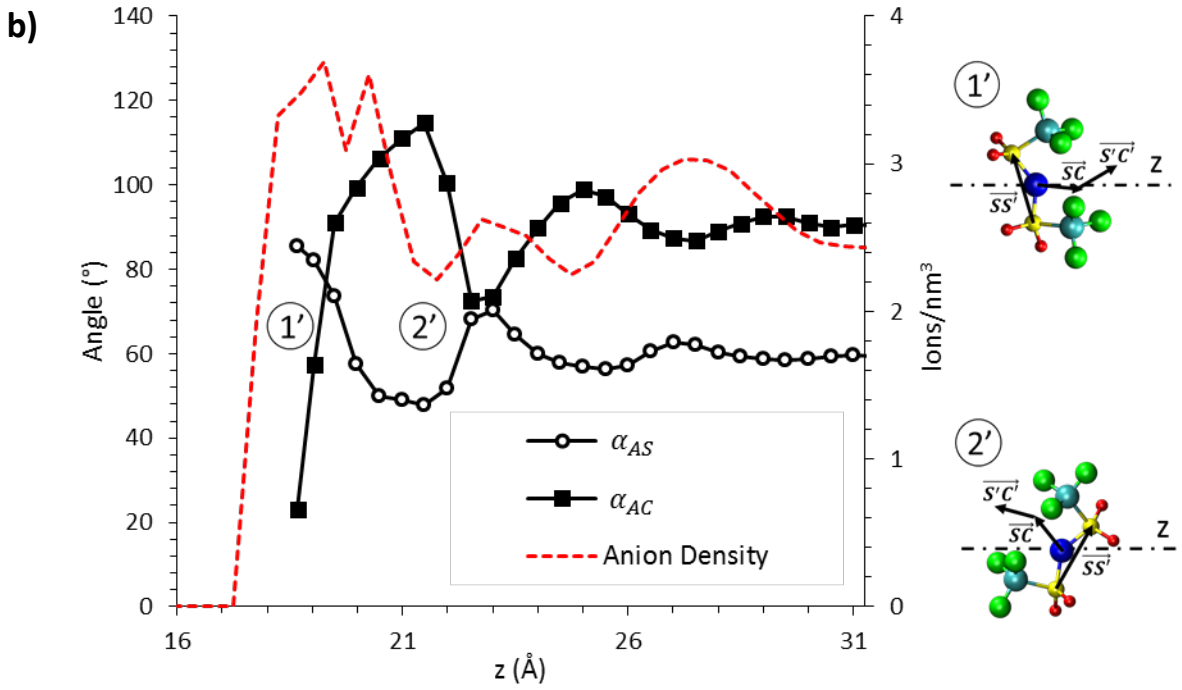

Figure 5. *Ions orientation close to the wall under confinement, at 350 K and 500 MPa. 7a) Cations orientation with respect to the surface: variation of α_{CR}, the average angle between the normal to the surfaces (z axis) and the vector normal to cation rings. The cation density profile is superimposed for comparison (blue dashed line). 7b) Anions and CF_3 orientations with respect to the z axis represented by the variation of α_{AS} and α_{AC} angles (see text for detail). The anion density profile is superimposed for comparison (red dashed line).*

Still considering Fig.4, the width of the density peaks should be correlated to the size of the molecules; nevertheless the width of the first [mmIm$^+$] and [NTf$_2^-$] density peaks was significantly different although the ions were of similar size. The organization of the molecules in the first layers nearby the surfaces provided an explanation, as it can be seen in Fig.5 where the orientation taken by the ions in that region is reported. Fig.5a shows the variation of α_{CR}, the average angle between the normal to the wall and the vectors normal to cation rings: a low α_{CR} value indicates that cations tend to be oriented parallel to the surface. Open circles on Fig.5b show the variation of α_{AS}, the average angle between the normal to the wall and the vectors $\overrightarrow{SS'}$ of the anions, S and S' being the two sulfur atoms. Similarly, black squares on Fig.5b display the variation vs. the distance from the wall of α_{AC}, the average angle between the normal to the solid-walls and the sum of the two vectors $\overrightarrow{SC}$ and $\overrightarrow{S'C'}$ of an anion, (S,S') and (C,C') being the couples of sulfur and carbon atoms,

respectively. From the last two cases, the closer to 90° the value of α_{AS} and the closer to 0° the value of α_{AC} are, the more the anions are oriented parallel to the surface with the CF_3 groups pointing toward the central part occupied by the IL.

Fig.5a and 5b show that, at the solid-liquid interface, both cations and anions were oriented parallel to the walls. Nevertheless, the CF_3 groups of the anions in contact with the walls were distinctly oriented perpendicular to the walls, which explains the broader density peak of the anions. These results are in accordance with the observations of two others research groups who studied the same [$mmIm^+$][NTf_2^-] IL pairs confined between either non-charged gold surfaces[19] or negatively-charged mica surfaces[41]. [$mmIm^+$] cations were found to be oriented parallel to mica surfaces and [NTf_2^-] anions oriented with their CF_3 group pointing toward the bulk. Other works carried out with different IL pairs presented comparable results regarding ions orientation. Atkin[18] and Mendonça[39] observed the following trends on graphite and iron surfaces, respectively: the cation rings tended to align parallel to the surfaces while the anions alkyl chains were oriented toward the bulk. However in the same study but on mica surfaces, Atkin observed a slightly different orientation of [$emIm^+$] cations with their alkyl chain pointing toward the bulk. The positive charge of the cations attracted by mica being located in the imidazolium ring, it was suggested that long alkyl-chains tend to get away from mica surfaces. Those tendencies were also confirmed through MD works[17] on confined [$emIm^+$][NTf_2^-].

Finally, combining our results with results from the literature, the layering structuration of the ions in confinement appears to strongly depend on the surface charge, with the formation of:

- separated cation and anion monolayers when confined between charged surfaces,
- mixed layers when confined between uncharged surfaces, either polar or nonpolar.

On the other hand, the orientation of IL ions is found to be less sensitive to the surface charge.

3.3 Confined ionic liquid: shearing

We then sheared the confined system by imposing opposite velocities of $\pm U/2$ to the confining walls (Fig.2b). The temperature was kept constant and equal to 350 K in the walls and was free to evolve in the fluid. The pressure applied to the system was held to p = 500 MPa. The shear velocity, U, was varied from 2.12 to 160 m/s, leading to apparent shear rates, $\dot{\gamma}_{app} = U/h$ (with h the IL thickness), ranging between ca. 8x10^{8} and 6x10^{10} s^{-1}. The global film thickness increased slightly but regularly with the shear velocity, up to ca. 7 % for the extreme case of U = 160 m/s. The structuration of the [mmIm^{+}][NTf$_2^{-}$] IL remained remarkably similar to the non-sheared one shown in Fig.4.

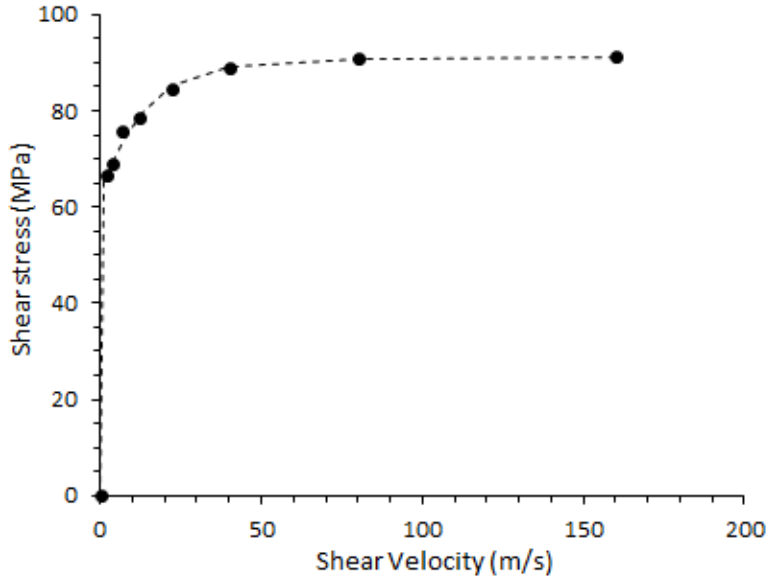

Figure 6. *Evolution of the global shear stress τ in the lubricated contact as a function of the shear velocity, for an imposed pressure of 500 MPa and a wall temperature of 350 K. The dashed line is a guide for the eyes. The shear velocity was varied between 2.12 and 160 m/s.*

Global response - We first measured the global response of the system: Fig.6 represents the evolution of the global shear stress $\tau = F_{\text{shear}}/A$ (with F_{shear} the total shear force measured on the confining walls and *A* the contact area) in the lubricated contact as a function of the shear velocity. The shear stress varied only slightly when the shear velocity spanned over almost 2 orders of magnitude, and reached a plateau at high shear velocities. The corresponding (solid) friction

coefficient, $\zeta = \tau / p$, ranged between 0.1 and 0.2, which is consistent with experimental measurements on nanoconfined IL[25,42].

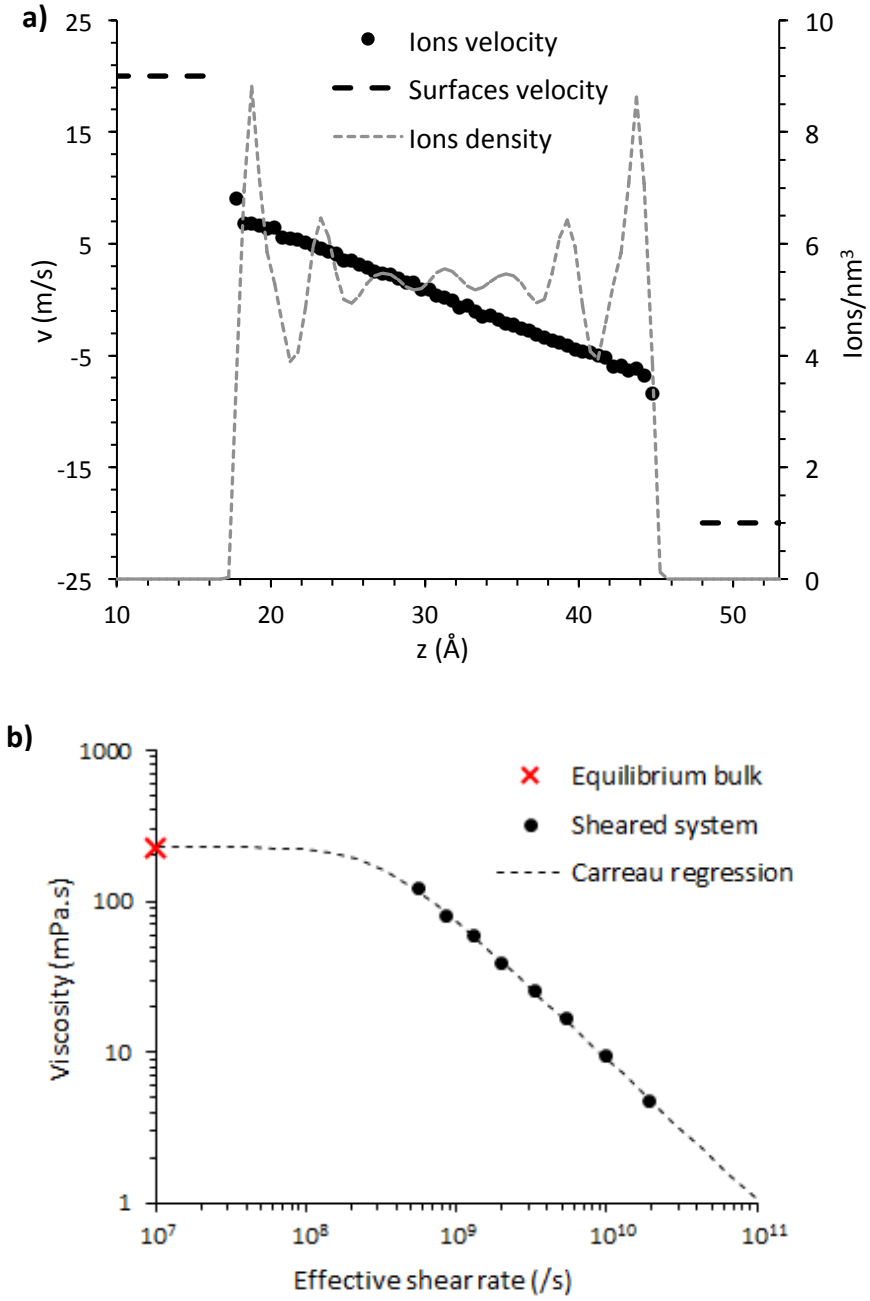

Figure 7. Confined [mmIm$^+$][NTf$_2^-$] ionic liquid undershear, for an imposed pressure of 500 MPa and a wall temperature of 350 K. 9a) Typical velocity profile (U = 40 m/s); the total density profile of the IL is superimposed for comparison. 9b) Viscosity of the confined IL as a function of the effective shear rate $\dot{\gamma}_{eff} = -dv/dz$ in the confined fluid. The dashed line is a Carreau regression of the viscosity. The red cross indicates the value of the Newtonian viscosity, obtained independently from equilibrium bulk simulations at 500 MPa and 350 K, using a Green-Kubo formula.

Local response: viscosity - In order to explain the saturation of the shear stress τ with the shear velocity, we then investigated the IL response locally. Fig.7a represents a typical velocity profile, obtained for a shear velocity of U = 40 m/s at a pressure of 500 MPa and a wall temperature of 350 K. Overall, the velocity profile was little affected by the IL layering close to the walls and remained linear throughout the whole fluid film. This homogeneity was not always ascertained with other fluids: a numerical study quantified the viscosity profiles of different Lennard-Jones fluids in confinement[43] and detected some viscosity reduction between well-formed layers near the surfaces. The strong interaction between the formed mixed layers in our study could explain the absence of similar variations.

The confined fluid then underwent a homogeneous effective shear rate, defined as $\dot{\gamma}_{eff} = -dv/dz$ in the linear region of the velocity profile. The rheology of the confined IL was characterized by computing the viscosity $\eta(\dot{\gamma}_{eff}) = \tau/\dot{\gamma}_{eff}$, as represented in Fig.7b. As for the bulk IL at ambient temperature and pressure, the evolution of the viscosity with the effective shear rate was well described by a Carreau law (Eq. 1), with a Newtonian viscosity η_N = 229 mPa.s, a relaxation time t_{rel} = 3.21 ns, and an exponent N = 0.517 (note that although the MD data did not reach the Newtonian plateau, the lowest effective shear rates simulated were sufficiently close to it so as to estimate the Newtonian viscosity with good accuracy). Remarkably, the Newtonian viscosity obtained from the Carreau fit matched the value obtained independently from equilibrium bulk simulations at 500 MPa and 350 K, using a Green-Kubo formula: 225 ± 17 mPa.s. However, the exponent *N* was significantly larger for the confined IL (*N* = 0.517, at a pressure of 500 MPa and a wall temperature of 350 K) than in bulk (*N* = 0.302, at a pressure of 0.1 MPa and a fluid temperature of 303 K).

Local response: liquid/solid slip - Remarkably, the velocity profiles also revealed the presence of a velocity jump at the interfaces between the IL and the oxide surfaces, a phenomenon referred to as liquid/solid slip[44] (Fig.7a). Hydrodynamic slip is described with the partial-slip boundary condition, which links the slip velocity v_{slip} (i.e. the velocity jump at the liquid/solid interface) to the shear rate

in the liquid at the solid surface. In a simple shear flow as considered here, the slip velocity is directly related to the effective shear rate in the liquid as follows:

$$v_{slip} = b \times \dot{\gamma}_{eff} \quad (3)$$

where b is the so-called slip length, which can be interpreted as the depth inside the wall where the linear extrapolation of the fluid velocity profile reaches the wall velocity[44]. For a given shear velocity, liquid/solid slip reduces the effective shear rate inside the IL, which can be expressed as:

$$\dot{\gamma}_{eff} = U/(h + 2b) = \dot{\gamma}_{app}/(1 + 2b/h) \quad (4)$$

where $\dot{\gamma}_{app} = U/h$.

Liquid/solid slip has therefore a significant influence on the effective shear rate when the slip length compares with the lubricating film width, as it was the case here.

To offer some insight into the origin of slip in the present system, it should be emphasized that the slip length, though it has a simple kinematic interpretation, is not a fundamental property of the liquid/solid interface. Indeed, the partial slip boundary condition (Eq. 3) stems physically from the identification of the bulk viscous shear stress in the liquid close to the wall:

$$\tau = \eta \times \dot{\gamma}_{eff} \quad (5)$$

with an interfacial liquid/solid friction stress :

$$\tau = \lambda \times v_{slip} \quad (6)$$

where λ is the liquid/solid friction coefficient[44–46]. Combining Eq. (5) and Eq. (6), one obtains the partial slip boundary condition Eq. (3), where the slip length is given by:

$$b = \eta/\lambda \quad (7)$$

The slip length is accordingly a combination of the bulk liquid viscosity and the interfacial friction coefficient.

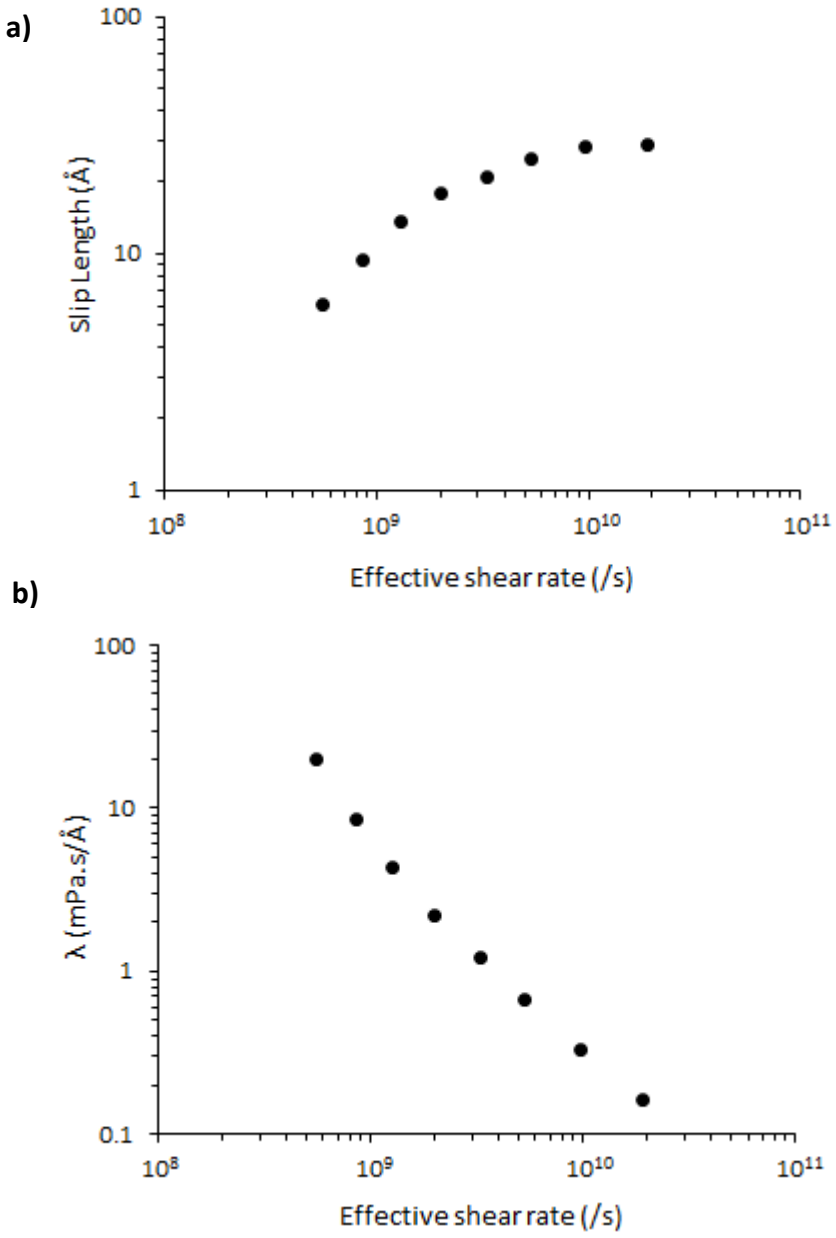

Figure 8. Effective shear rate dependence of a) the slip length $b = v_{slip}/\dot{\gamma}_{eff}$ *and b) the liquid/solid friction coefficient* $\lambda = \tau/v_{slip}$ *at the IL/FeO interface (p = 500 MPa and wall temperature T = 350 K).*

Fig.8 shows the evolution of both the slip length b and the liquid/solid friction coefficient λ as a function of the effective shear rate. To the best of our knowledge, no hydrodynamic slip has been observed experimentally with ionic liquids. However, previous studies on alkanes confined between various non-polar surfaces identified wall-slip occurrence and its strong relationship with the surface composition and orientation[10]. Depending on the atom nature of the solid body in contact with the fluid, the commensurability and the corrugation forces at the interface can

profoundly change, and directly influence the presence and intensity of wall slip[10,45,46]. Oxygen and iron atoms (both present at the interface of the IL/oxide system of the current study) present Lennard-Jones energy coefficients[32] favoring wall slip in the absence of Coulombic interactions[10]. Nevertheless, when considering ionic liquids, Coulombic interactions are predominant at the interface and should modify the corrugation forces opposed to slip. Other MD works simulating different confined ILs encountered little to no slip response to shearing[23,47]. In order to understand the origin of slip in the current study, it became essential to characterize the solid/liquid interactions. In particular, for simple liquids at low pressure and small shear rate (i.e. in the linear response regime), a large experimental and numerical effort over the last 20 years has highlighted the existence of a quasi-universal relationship between the slip length and the wetting properties of the liquid/solid couple[43,48], although some recent works have shown that the wetting properties alone can fail to predict the slip length[49,50]. This quasi-universal relationship predicts that slippage is favored on non-wetting substrates, and that it should not occur for contact angles below ca. 80°. We therefore measured the wetting properties of the IL/FeO couple in an independent simulation of an IL droplet on a FeO substrate and found a rather wetting behavior, with a contact angle of 43°. Hence, the relationship between wetting and slippage fails for the system under consideration, which suggests that the presence of slip in our study was due to the particular working conditions of high pressure and high shear rates typical of a lubricated contact. Specifically, the combination of two factors can explain the presence of significant slip. Firstly, the important viscosity resulting from the severe confinement of the system (up to 225mPa.s at p = 500 MPa) tends to increase the slip length as the two values are directly proportional (Eq. 7). Secondly, the comparison of the evolution with the shear rate of both the bulk viscosity and the fluid/solid friction coefficient reveals that the first decreases slower than the second, resulting in an increase of the slip length with the shear rate (Eq. 7). In other words, the strong viscosity of the fluid has a higher influence on slip than the friction of the fluid/solid interface.

Another interesting feature concerns the fact that the slip length saturated in the large shear rate limit. This contrasts with previous numerical results on simple fluids obtained in less severe thermodynamic conditions, where the slip length has been shown to diverge[51], although other works also observed a saturation when using thermostated walls[52,53]. Back to Fig.8b, in the high

shear rate limit λ scaled exactly as the fluid viscosity. Consequently, the slip length, which is the ratio between the two quantities, reached a constant value. In other words, the vanishing liquid/solid friction at high shear rates did not result in a diverging slip length because it was exactly compensated by the vanishing fluid viscosity.

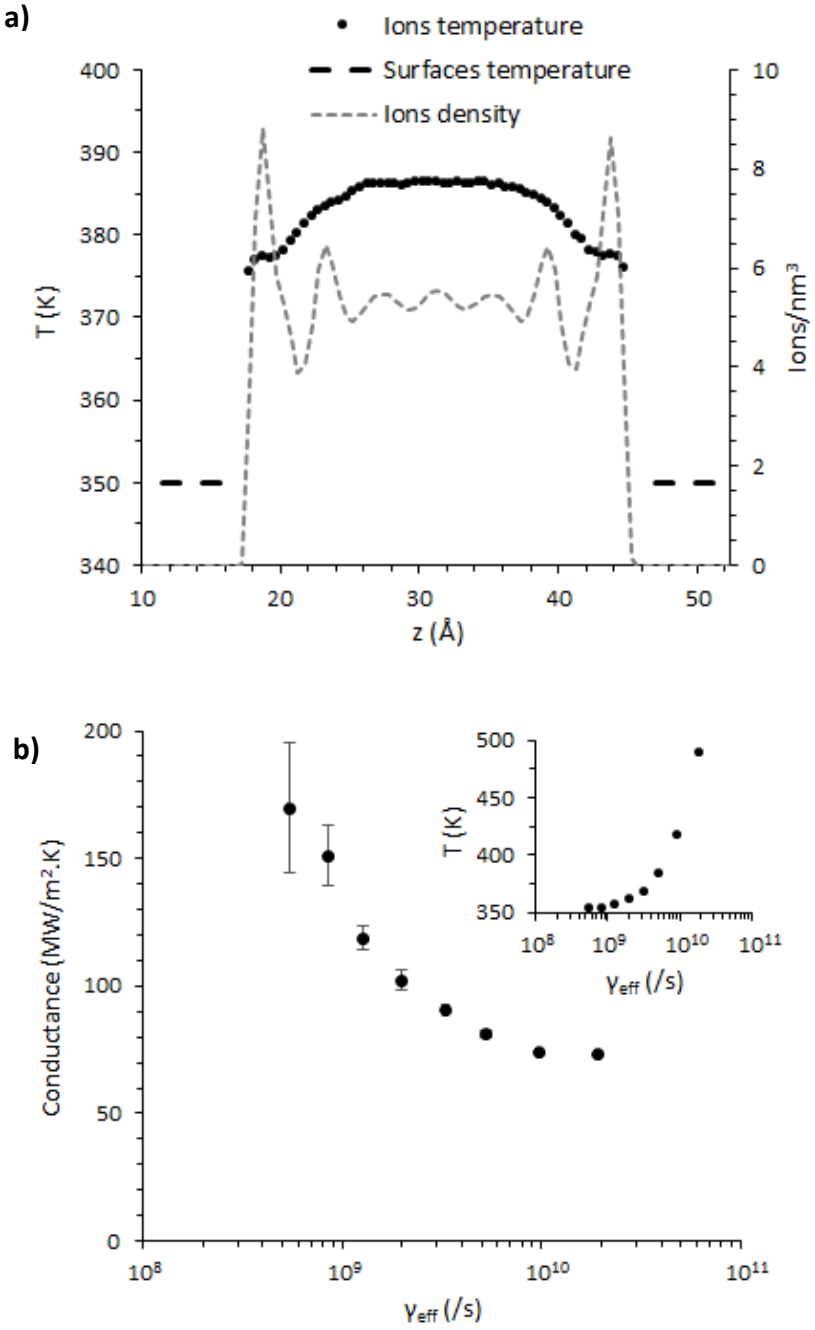

Figure 9. (a) Typical temperature profile of the sheared IL, for a shear velocity U = 40 m/s, a pressure p = 500 MPa, and a wall temperature T =350 K. (b) Evolution of the thermal conductance of the fluid/solid interface with the effective shear rate. Inset: Evolution of the average temperature of the confined IL with the effective shear rate.

Local response: temperature slippage - As it can be observed in Fig.9a, showing a typical velocity profile, a thermal slip operated simultaneously to the one of velocity, associated with a finite thermal conductance of the liquid/solid interface. Fig.9b represents the evolution of the thermal conductance $G = q/\Delta T$ (with q the heat flux and ΔT the temperature jump at the liquid/solid interface) as a function of the effective shear rate in the IL. The variation of the conductance appeared to be strongly correlated to the inverse of the evolution of the slip length (Fig.9a). This is consistent with previous observations[54] of a correlation between hydrodynamic and thermal slips, and could result from shared underlying mechanisms occurring at the molecular level.

As a consequence of the limited heat transfer between the lubricant and the walls, the average temperature of the confined fluid increased progressively and significantly with the effective shear rate, as shown in the inset of Fig.9b. This temperature increase is the key to the specific behavior of the confined IL. In particular, it explains the observed increase of the lubricant film thickness with the shear velocity, through thermal expansion of the fluid. More importantly, the increase of fluid temperature is expected to amplify the decrease of viscosity with the shear rate, explaining the larger exponent *N* in the Carreau law measured for the confined fluid, as compared to the bulk one. One can note here that the Carreau law for the confined fluid is therefore an effective one, hiding a complex mechanism involving the coupling between the fluid temperature and the shear rate.

Back to the global response – Now that we have investigated in detail the bulk and interfacial response of the confined IL to shear, we will show that the saturation of the global shear stress (Fig.6) can be related to the particular rheology of the confined IL, measured inside the lubricated contact. We will also emphasize that due to this particular rheology, the presence of liquid/solid slip has no significant influence on the plateau value of the global shear stress.

Indeed, the global shear stress in the lubricated contact can be expressed as the viscous shear stress inside the fluid: $\tau = \eta_{eff} \times \dot{\gamma}_{eff}$. We have shown that the viscosity of the confined IL followed a Carreau law (Eq. 1), with an exponent N = 0.517. Beyond the Newtonian plateau (i.e. when $\dot{\gamma}_{eff} \gg 1/t_{rel}$), the Carreau law simplifies to a simple power law:

$$\eta_{(\dot{\gamma}_{eff})} \sim \eta_N \times \left(\dot{\gamma}_{eff} \times t_{rel}\right)^{\frac{N-1}{N}}$$

The shear stress in the IL then becomes: $\sim \eta_N \times t_{rel}^{\frac{N-1}{N}} \times \dot{\gamma}_{eff}^{\frac{N-1}{N}+1}$. For an exponent of precisely 0.5, τ becomes independent of the effective shear rate, and reaches a plateau at a value: $\tau_{max} \sim \eta_N / t_{rel}$. Remarkably, in that specific situation, the reduction of effective shear rate due to liquid/solid slip will therefore not help to reduce the global shear stress.

Beyond the interest of previous results for the chemical physics community, the response of the system to shearing give some insight on the choice of using ILs as lubricants in steel-steel contacts under severe working conditions. As the shear rate rises, this work revealed that the presence of both an anomalous effective shear thinning and a velocity wall slip lead to a limitation of the shear stress and thus of the global friction. It is important to notice that this friction limitation is accompanied by a significant temperature increase. In that regard, the high thermal stability of ILs (and especially of the [mmIm$^+$][NTf$_2^-$] compound) makes them particularly suitable lubricants compared with conventional ones.

Conclusion

Molecular dynamics (MD) simulations were used to quantitatively describe the structure and dynamics of a [mmIm$^+$][NTf$_2^-$] ionic liquid (IL) confined between two FeO surfaces. Several features occurring in the system were thus characterized: (i) viscosity - shear rate dependency (ii), layering structuration similar to the one found with uncharged surfaces and standard ions orientation, (iii) wall slip and low interfacial friction, (iv) thermal slip and its consequence on the previous points.

Overall, this article provides a methodology for accurate modeling of the tribological contact lubricated by a nanometer-thick IL lubricant. In particular, it shows the importance of accounting for heat transfer, which can profoundly modify the mechanical response of the lubricated contact. The results emphasize the rich phenomenology arising in typical working conditions of a lubricated contact, involving extreme pressure and temperature, together with large shear rates, pushing the system beyond the linear response regime traditionally considered in the physics community.

Further works are needed to fully outline the ionic liquid response to shearing under severe confinement. Firstly, the ultimate reduction of the entrapped fluid inside nano-contacts modeled by IL films of 1-3 layers could reveal interesting properties like solid-like behavior[24]. Secondly, brute-

force non-equilibrium MD simulations such as the ones used in this work are limited by thermal noise at low shear velocity. Here advanced techniques such as the transient time correlation function method[55] could override this limitation and be used to probe the non-linear response of confined IL down to the Newtonian regime. Finally, accurate models such as the one used in this work could help investigate more quantitatively friction control through external fields in IL-lubricated contacts[56,57].

Acknowledgments

The authors are grateful to the SKF company for financial support through the Research Chair "Lubricated Interfaces for the future" hosted by the INSA de Lyon Foundation. Guillermo E. Morales-Espejel is acknowledged for his much appreciated expertise on lubrication systems. Our last thanks go to the Fédération Lyonnaise de Modélisation et Sciences Numériques (FLMSN) for providing computing resources via the P2CHPD facility.

References

(1) Dold, C.; Amann, T.; Kailer, A. Influence of Structural Variations on Imidazolium-Based Ionic Liquids. *Lubr. Sci.* **2013**, *25*, 251–268.

(2) Maginn, E. J. Molecular Simulation of Ionic Liquids Current Status and Future Opportunities. *J. Phys. Condens. Matter* **2009**, *21*, 17.

(3) Zhou, F.; Liang, Y.; Liu, W. Ionic Liquid Lubricants: Designed Chemistry for Engineering Applications. *Chem. Soc. Rev.* **2009**, *38*, 2590–2599.

(4) Palacio, M.; Bhushan, B. A Review of Ionic Liquids for Green Molecular Lubrication in Nanotechnology. *Tribol. Lett.* **2010**, *40*, 247–268.

(5) Minami, I. Ionic Liquids in Tribology. *Molecules* **2009**, *14*, 2286–2305.

(6) Bermúdez, M.-D.; Jiménez, A.-E.; Sanes, J.; Carrión, F.-J. Ionic Liquids as Advanced Lubricant Fluids. *Molecules* **2009**, *14*, 2888–2908.

(7) Fernández, J.; Paredes, X.; Gaciño, F. M.; Comuñas, M. J. P.; Pensado, A. S. Pressure-Viscosity Behaviour and Film Thickness in Elastohydrodynamic Regime of Lubrication of Ionic Liquids and Other Base Oils. *Lubr. Sci.* **2013**, *nc*, n/a – n/a.

(8) Morales, W.; Street, K. W.; Richard, R. M.; Valco, D. J. Tribological Testing and Thermal Analysis of an Alkyl Sulfate Series of Ionic Liquids for Use as Aerospace Lubricants. *Tribol. Trans.* **2012**, *55*, 815–821.

(9) Dowson, D. *History of Tribology*; Longman: London, 1979.

(10) Savio, D.; Fillot, N.; Vergne, P.; Zaccheddu, M. A Model for Wall Slip Prediction of Confined N-Alkanes: Effect of Wall-Fluid Interaction Versus Fluid Resistance. *Tribol. Lett.* **2012**, *46*, 11–22.

(11) Pensado, A. S.; Comuñas, M. J. P.; Fernández, J. The Pressure-Viscosity Coefficient of Several Ionic Liquids. *Tribol. Lett.* **2008**, *31*, 107–118.

(12) Amann, T.; Dold, C.; Kailer, A. Rheological Characterization of Ionic Liquids and Ionic Liquid Crystals with Promising Tribological Performance. *Soft Matter* **2012**, *8*, 9840–9846.

(13) Masuko, M.; Terawaki, T.; Kobayashi, K.; Aoki, S.; Suzuki, A.; Fujinami, Y.; Nogi, T.; Obara, S. Contrasting Lubrication Properties of Imidazolium-Based Ionic Liquids Affected by the Nature of the Surface Under High Vacuum. *Tribol. Lett.* **2014**, *55*, 235–244.

(14) López Sánchez, F.; Otero, I.; López, E. R.; Fernández, J. Tribological Properties of Two Bis(trifluoromethylsulfonyl)imide-Based Ionic Liquids on Steel-Steel Contact. *Tribol. Trans.* **2014**, *57*, 637–646.

(15) Perkin, S.; Albrecht, T.; Klein, J. Layering and Shear Properties of an Ionic Liquid, 1-Ethyl-3-Methylimidazolium Ethylsulfate, Confined to Nano-Films between Mica Surfaces. *Phys. Chem. Chem. Phys.* **2010**, *12*, 1243–1247.

(16) Somers, A. E.; Howlett, P. C.; MacFarlane, D. R.; Forsyth, M. A Review of Ionic Liquid Lubricants. *Lubricants* **2013**, *1*, 3–21.

(17) Rajput, N. N.; Monk, J.; Hung, F. R. Structure and Dynamics of an Ionic Liquid Confined Inside a Charged Slit Graphitic Nanopore. *J. Phys. Chem. C* **2012**, *116*, 14504–14513.

(18) Atkin, R.; Warr, G. G. Structure in Confined Room-Temperature Ionic Liquids. *J. Phys. Chem. C* **2007**, *111*, 5162–5168.

(19) Cremer, T.; Stark, M.; Deyko, A.; Steinrück, H.-P.; Maier, F. Liquid/Solid Interface of Ultrathin Ionic Liquid Films: [C1C1Im][Tf2N] and [C8C1Im][Tf2N] on Au(111). *Langmuir* **2011**, *27*, 3662–3671.

(20) Perkin, S.; Crowhurst, L.; Niedermeyer, H.; Welton, T.; Smith, A. M.; Gosvami, N. N. Self-Assembly in the Electrical Double Layer of Ionic Liquids. *Chem. Commun.* **2011**, *47*, 6572–6574.

(21) Federici Canova, F.; Matsubara, H.; Mizukami, M.; Kurihara, K.; Shluger, A. L. Shear Dynamics of Nanoconfined Ionic Liquids. *Phys. Chem. Chem. Phys.* **2014**, *16*, 8247–8256.

(22) Pinilla, C.; Del Pópolo, M. G.; Lynden-Bell, R. M.; Kohanoff, J.; Pópolo, M. Del. Structure and Dynamics of a Confined Ionic Liquid. Topics of Relevance to Dye-Sensitized Solar Cells. *J. Phys. Chem. B* **2005**, *109*, 17922–17927.

(23) Mendonça, A. C. F.; Padua, A. A. H.; Malfreyt, P. Nonequilibrium Molecular Simulations of New Ionic Lubricants at Metallic Surfaces: Prediction of the Friction. *J. Chem. Theory Comput.* **2013**, *9*, 1600–1610.

(24) Perkin, S. Ionic Liquids in Confined Geometries. *Phys. Chem. Chem. Phys.* **2012**, *14*, 5052–5062.

(25) Espinosa-Marzal, R. M.; Arcifa, A.; Rossi, A.; Spencer, N. D. Ionic Liquids Confined in Hydrophilic Nanocontacts: Structure and Lubricity in the Presence of Water. *J. Phys. Chem. C* **2014**, *118*, 6491–6503.

(26) Canongia Lopes, J. N.; Pádua, A. A. H. Molecular Force Field for Ionic Liquids Composed of Triflate or Bistriflylimide Anions. *J. Phys. Chem. B* **2004**, *108*, 16893–16898.

(27) Canongia Lopes, J. N.; Deschamps, J.; Pádua, A. A. H. Modeling Ionic Liquids Using a Systematic All-Atom Force Field. *J. Phys. Chem. B* **2004**, *108*, 2038–2047.

(28) Salanne, M. Simulations of Room Temperature Ionic Liquids: From Polarizable to Coarse-Grained Force Fields. *Phys. Chem. Chem. Phys.* **2015**, *17*, 14270–14279.

(29) Schroder, C. Comparing Reduced Partial Charge Models with Polarizable Simulations of Ionic Liquids. *Phys. Chem. Chem. Phys.* **2012**, *14*, 3089–3102.

(30) Chaban, V. Polarizability versus Mobility: Atomistic Force Field for Ionic Liquids. *Phys. Chem. Chem. Phys.* **2011**, *13*, 16055–16062.

(31) Gräfen, H.; Horn, E.-M.; Schlecker, H.; Schindler, H. Corrosion. In *Ullmann's Encyclopedia of Industrial Chemistry*; Wiley-VCH Verlag GmbH & Co. KGaA, 2000.

(32) Cygan, R. T.; Liang, J.-J.; Kalinichev, A. G. Molecular Models of Hydroxide, Oxyhydroxide, and Clay Phases and the Development of a General Force Field. *J. Phys. Chem. B* **2004**, *108*, 1255–1266.

(33) Phan, A.; Ho, T. A.; Cole, D. R.; Striolo, A. Molecular Structure and Dynamics in Thin Water Films at Metal Oxide Surfaces: Magnesium, Aluminum, and Silicon Oxide Surfaces. *J. Phys. Chem. C* **2012**, *116*, 15962–15973.

(34) Plimpton, S. Fast Parallel Algorithms for Short-Range Molecular Dynamics. *J. Comput. Phys.* **1995**, *117*, 1–19.

(35) Tuckerman, M.; Berne, B. J.; Martyna, G. J. Reversible Multiple Time Scale Molecular Dynamics. *J. Chem. Phys.* **1992**, *97*, 1990–2001.

(36) Allen, M. P.; Tildesley, D. J. *Computer Simulation of Liquids*; Oxford university press, 1989.

(37) Müller-Plathe, F. Reversing the Perturbation in Nonequilibrium Molecular Dynamics: An Easy Way to Calculate the Shear Viscosity of Fluids. *Phys. Rev. E* **1999**, *59*, 4894–4898.

(38) Bair, S. A Rough Shear-Thinning Correction for EHD Film Thickness. *STLE Trib. Trans.* **2004**, *47*, 361–365.

(39) Mendonça, A. C. F.; Malfreyt, P.; Pádua, A. A. H. Interactions and Ordering of Ionic Liquids at a Metal Surface. *J. Chem. Theory Comput.* **2012**, *8*, 3348–3355.

(40) Sweeney, J.; Webber, G. B.; Rutland, M. W.; Atkin, R. Effect of Ion Structure on Nanoscale Friction in Protic Ionic Liquids. *Phys. Chem. Chem. Phys.* **2014**, 16651–16658.

(41) Deyko, A.; Cremer, T.; Rietzler, F.; Perkin, S.; Crowhurst, L.; Welton, T.; Steinrück, H.-P.; Maier, F. Interfacial Behavior of Thin Ionic Liquid Films on Mica. *J. Phys. Chem. C* **2013**, *117*, 5101–5111.

(42) Smith, A. M.; Lovelock, K. R. J.; Gosvami, N. N.; Welton, T.; Perkin, S. Quantized Friction across Ionic Liquid Thin Films. *Phys. Chem. Chem. Phys.* **2013**, *15*, 15317–15320.

(43) Hoang, H.; Galliero, G. Local Viscosity of a Fluid Confined in a Narrow Pore. *Phys. Rev. E* **2012**, *86*, 21202.

(44) Bocquet, L.; Barrat, J.-L. Flow Boundary Conditions from Nano- to Micro-Scales. *Soft Matter* **2007**, *3*, 685–693.

(45) Falk, K.; Sedlmeier, F.; Joly, L.; Netz, R. R.; Bocquet, L. Molecular Origin of Fast Water Transport in Carbon Nanotube Membranes: Superlubricity versus Curvature Dependent Friction. *Nano Lett.* **2010**, *10*, 4067–4073.

(46) Falk, K.; Sedlmeier, F.; Joly, L.; Netz, R. R.; Bocquet, L. Ultralow Liquid/solid Friction in Carbon Nanotubes: Comprehensive Theory for Alcohols, Alkanes, OMCTS, and Water. *Langmuir* **2012**, *28*, 14261–14272.

(47) Castejón, H. J.; Wynn, T. J.; Marcin, Z. M. Wetting and Tribological Properties of Ionic Liquids. *J. Phys. Chem. B* **2014**, *118*, 3661–3668.

(48) Huang, D. M.; Sendner, C.; Horinek, D.; Netz, R. R.; Bocquet, L. Water Slippage versus Contact Angle: A Quasiuniversal Relationship. *Phys. Rev. Lett.* **2008**, *101*, 226101.

(49) Ho, T. A.; Papavassiliou, D. V; Lee, L. L.; Striolo, A. Liquid Water Can Slip on a Hydrophilic Surface. *Proc. Natl. Acad. Sci. U. S. A.* **2011**, *108*, 16170–16175.

(50) Tocci, G.; Joly, L.; Michaelides, A. Friction of Water on Graphene and Hexagonal Boron Nitride from Ab Initio Methods: Very Different Slippage Despite Very Similar Interface Structures. *Nano Lett.* **2014**, *14*, 6872–6877.

(51) Thompson, P. A.; Troian, S. M. A General Boundary Condition for Liquid Flow at Solid Surfaces. *Nature* **1997**, *389*, 360–362.

(52) Martini, A.; Hsu, H. Y.; Patankar, N. A.; Lichter, S. Slip at High Shear Rates. *Phys. Rev. Lett.* **2008**, *100*, 1–4.

(53) Martini, A.; Roxin, A.; Snurr, R. Q.; Wang, Q.; Lichter, S. Molecular Mechanisms of Liquid Slip. *J. Fluid Mech.* **2008**, *600*, 257–269.

(54) Barrat, J.-L.; Chiaruttini, F. F. Kapitza Resistance at the Liquid Solid Interface. *Mol. Phys.* **2003**, *101*, 1605–1610.

(55) Bernardi, S.; Brookes, S. J.; Searles, D. J.; Evans, D. J. Response Theory for Confined Systems. *J. Chem. Phys.* **2012**, *137*, -.

(56) Li, H.; Wood, R. J.; Rutland, M. W.; Atkin, R. An Ionic Liquid Lubricant Enables Superlubricity to Be “Switched on” in Situ Using an Electrical Potential. *Chem. Commun. (Camb).* **2014**, *50*, 4368–4370.

(57) Fajardo, O. Y.; Bresme, F.; Kornyshev, A. A.; Urbakh, M. Electrotunable Lubricity with Ionic Liquid Nanoscale Films. *Sci. Rep.* **2015**, *5*, 7698.